Catal Lett (2013) 143:539–546
DOI 10.1007/s10562-013-1006-6

Palladium Nanoparticle–Graphene Catalysts for Asymmetric Hydrogenation

Kornél Szőri · Robert Puskás · György Szőllősi · Imre Bertóti · János Szépvölgyi · Mihály Bartók

Abstract We report for the first time the application of palladium nanoparticle-graphene (Pd/Gn) catalysts in the asymmetric hydrogenation of aliphatic α,β-unsaturated carboxylic acids using cinchonidine as chiral modifier. Pd/Gns were prepared by deposition–precipitation from the aqueous phase over graphite oxide and subsequent simultaneous reduction of both the support and the metal precursor with $NaBH_4$. The materials obtained were characterized by ICP optical emission spectroscopy, X-ray diffraction spectroscopy, Raman spectroscopy, transmission electron microscopy and X-ray photoelectron spectroscopy. We demonstrate that the Pd/Gns modified by cinchonidine can act as efficient catalysts in the asymmetric hydrogenation of α,β-unsaturated carboxylic acids for producing optically enriched saturated carboxylic acids.

Keywords Carboxylic acid · Cinchona alkaloid · Enantioselective · Graphene · Hydrogenation · Palladium

K. Szőri · G. Szőllősi (✉) · M. Bartók (✉)
MTA-SZTE Stereochemistry Research Group, Hungarian Academy of Sciences, Dóm tér 8, Szeged 6720, Hungary
e-mail: szollosi@chem.u-szeged.hu

M. Bartók
e-mail: bartok@chem.u-szeged.hu

R. Puskás
Department of Applied and Environmental Chemistry, University of Szeged, Rerrich Béla tér 1, Szeged 6720, Hungary

I. Bertóti · J. Szépvölgyi
Institute of Materials and Environmental Chemistry, Research Centre of Natural Sciences, Hungarian Academy of Sciences, Pusztaszeri út 59-67, Budapest 1025, Hungary

J. Szépvölgyi
Research Institute of Chemical and Process Engineering, Faculty of Information Technology, University of Pannonia, Egyetem utca 2, Veszprém 8200, Hungary

M. Bartók
Department of Organic Chemistry, University of Szeged, Dóm tér 8, Szeged 6720, Hungary

1 Introduction

The application of heterogeneous catalytic methods in organic chemistry has become one of the most intensively researched areas [1–4]. Among these methods, procedures with the longest history are hydrogenations [5–7], which are mainly catalyzed by supported metals. In the course of the decades various supported metal catalysts have been developed with the purpose of achieving high activity and selectivity. Since supports have to meet a number of special requirements, in addition to generally used supports (activated carbon, SiO_2, Al_2O_3 and later zeolites and mesoporous materials) the development of other types of metal catalysts has also gained increased importance. The University of Szeged has also joined this line of research, with work on the use of amorphous metal alloys [8–10], layered materials such as clays [11–14] and graphimets [15–19].

In spite of the novel observations made, these studies did not lead to the expected results, especially in the case of graphimets. The reason for this was that the interlamellar space of graphimets with two dimensional (2-D) plane structure is not penetrated even by low-molecular-weight organic compounds. The discovery of graphene (Gn) [20], however, opened the way to the synthesis and study of catalysts consisting of metal nanoparticles supported by graphene in the hydrogenation of organic compounds as well [21–24]. Our research initiated in this field may be considered as the continuation of our earlier studies.

Special attention is given to the heterogeneous enantioselective hydrogenation of prochiral organics resulting in optically active chiral building blocks used in the syntheses of pharmaceuticals, fragrances and agrochemicals [25–28]. To our knowledge, the application of metal-graphene nanocomposites in the asymmetric hydrogenation of prochiral compounds has not yet been attempted. The objective of the present work was the synthesis and characterization of Pd nanoparticle/graphenes (Pd/Gns) and their study in asymmetric hydrogenation reactions in the presence of cinchonidine modifier. Based on our earlier experience, we chose prochiral aliphatic α,β-unsaturated carboxylic acids as substrates for studying enantioselective hydrogenations [29–32] (Fig. 1), because it had been earlier confirmed that, these acids can be hydrogenated at moderate enantioselectivities over Pd catalysts to produce saturated acid chiral building blocks.

2 Experimental

2.1 Materials

Graphite powder (Aldrich 496588: <150 μm, 99.99 + %), $PdCl_2$ (Aldrich, ≥99.9 %), cinchonidine (CD, Alfa Aesar), the unsaturated carboxylic acids: (*E*)-2-methyl-2-hexenoic acid (**1a**, Alfa Aesar, 98 %), (*E*)-2-methyl-2-butenoic acid (**2a**, Aldrich, 98 %), itaconic acid (**3a**, Aldrich, ≥99 %), benzylamine (BA, Fluka, ≥99.5 %), high purity solvents and reagents (Aldrich and Scharlau Chemie) were used as received. Sodium borohydride and H_2 gas (Linde AG) of 99.999 % were used for catalyst reductions and in hydrogenations. Graphite oxide (GrO) was prepared by slight modification of the Hummers method [33].

2.2 Preparation of Palladium Nanoparticle–Graphene Hybrid Catalysts (Pd/Gn1, Pd/Gn2, Pd/Gn3) [34]

Pd/Gn1: 1 g of GrO was exfoliated into graphene oxide (GO) by sonication (Branson 1510 MT) in 250 cm^3 of water for 2 h. To prepare a catalyst containing around 5 % Pd a solution of 88 mg of $PdCl_2$ in 50 cm^3 of distilled water acidified with 0.072 cm^3 of conc HCl was added to the GO dispersion, followed by sonication for 30 min.

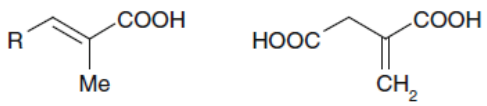

R = Pr (**1a**); R = Me (**2a**) (**3a**)

Fig. 1 Selected unsaturated carboxylic acids

Reduction was initiated by the addition of 724.4 mg of $NaBH_4$ freshly dissolved in 20 cm^3 of distilled water to the slurry cooled in ice bath and stirred magnetically. After 5 min, cooling was stopped and the mixture was stirred at room temperature for another 4 h. Next the solid material was centrifuged (Sigma 2-16 P; 5 min/10,000 rpm), washed with water and methanol three times (20 cm^3 each) and dried at 323 K for 12 h in a vacuum desiccator.

Pd/Gn2: 1 g of GrO and 2.54 g of Na_2CO_3 were mixed in 250 cm^3 distilled water, and the dispersion was sonicated for 1 h. 88 mg of $PdCl_2$ and 1.2 cm^3 of conc HCl dissolved in 21 cm^3 of distilled water were next added to the mixture chilled on ice and continuously stirred, followed by stirring at room temperature for 20 h. Reduction by $NaBH_4$ and isolation of Pd/Gn2 were carried out as described for Pd/Gn1.

Pd/Gn3: 1 g of GrO was exfoliated into GO by sonication in 250 ml of water for 2 h. Graphene (Gn) was next obtained by chemical reduction using $NaBH_4$ and isolation by centrifugation as described above for Pd/Gn1. Pd/Gn3 was then prepared from Gn using the method and the conditions described above for Pd/Gn2 (i.e. addition of Na_2CO_3 aq, $PdCl_2$ aq + conc HCl and finally $NaBH_4$ aq).

2.3 Characterization of the Palladium Nanoparticle/Graphene Catalysts

Inductively coupled plasma optical emission spectroscopy (ICP-OES) analysis were performed on a AMETEK produced Spectro Genesis EOP II type spectrometer after leaching the soluble constituents of the catalyst samples in warmed HCl + conc HNO_3 mixture and diluting the solutions. The transmission electron microscopy (TEM) investigations were carried out using Philips CM10 (100 kV) transmission electron microscope. The sample preparation involved mechanical grinding of the material and gluing the powder on a Cu TEM-grid. X-ray powder diffraction (XRD) analysis was effectuated on a Rigaku Miniflex-II diffractometer utilizing Cu Kα radiation. Raman spectra were the average of 256 scans measured at 4 cm^{-1} resolution on a Thermo Scientific DXR Raman microscope operating with 780 nm laser excitation of 5 mW power. X-ray photoelectron spectra (XPS) were recorded on a Kratos XSAM 800 spectrometer operated at fixed analyser transmission mode using Mg $K\alpha_{1,2}$ (1,253.6 eV) excitation. Wide scan spectra were recorded for all samples in the 100–1,300 eV kinetic energy range. Spectra were referenced to the energy of the C1s line of the polymeric or hydrocarbon type adventitious carbon, present at the surface of the samples, set at 284.8 ± 0.1 eV binding energy (BE) [35]. Chemical states of the constituent elements were determined with ±0.2 eV accuracy, and assigned by using available references. Quantitative analysis, based on peak area intensities (after removal of the Shirley-

type background), was performed by the Vision 2000 program using experimentally determined photo-ionisation cross-section data.

2.4 Catalytic Hydrogenation and Product Analysis

Hydrogenations were carried out in stainless steel autoclave equipped with glass liner. Under typical conditions 15 mg catalyst, 10 cm^3 toluene (or methanol in the hydrogenations of **3a**) were loaded into reactor, the autoclave was flushed with H_2, filled to 5 MPa. After 30 min pre-hydrogenation the given amount of modifier, substrate (**1a** or **2a** or **3a**) and BA additive were loaded into reactor, the autoclave was flushed with H_2, filled to the given H_2 pressure and the reaction was commenced by stirring the slurry using magnetic agitation (1000 rpm) at room temperature (297 K). After 90 min the H_2 was released, the slurry was filtered, the solution was treated with 10 % HCl aq. solution (except **3a**), dried over Na_2SO_4 and analyzed. Products obtained in hydrogenations of **3a** were transformed in dimethyl esters as previously described [30].

Products were identified by GC–MS analysis using Agilent Techn. 6890 N GC–5973 MSD equipped with 60 m HP-1MS capillary column. Conversions and enantioselectivities were calculated from gas chromatographic analysis using the formulae: Conv (%) = 100 × ([*S*] + [*R*]) / $[Acid]_0$; ee (%) = 100 × ([*S*] − [*R*] I/ ([*S*] + [*R*]) where $[Acid]_0$ is the initial concentration of the unsaturated acid (**1a**, **2a** or **3a**); [*S*] and [*R*] are the concentrations of the product enantiomers determined by gas-chromatographic analysis using Agilent Techn. 6890 N GC–FID instrument equipped with HP-Chiral (30 m × 0.25 mm, J&W Scientific Inc. for **1a** and **2a**) or Cyclosil-B (30 m × 0.25 mm; J&W Scientific Inc. for **3a**) chiral capillary columns. The analysis conditions were: head pressure 135 kPa He; column temperature: 358 K, retention times (min): (*S*)-**1b** 13.0, (*R*)-**1b** 13.9, **1a** 21.2; head pressure 135 kPa He; 388 K, retention times (min): (*S*)-**2b** 20.2, (*R*)-**2b** 21.8, **2a** 26.8; and head pressure 135 kPa He; 388 K, retention times of the corresponding dimethyl esters (min): (*S*)-**3b** 26.8, (*R*)-**3b** 27.7, **3a** 41.6. The absolute configuration of enantiomers were determined by GC analysis using commercially available optically pure products. Repeating some experiments three times resulted in product compositions reproducible within ±1 %.

3 Results and Discussions

The syntheses of Pd nanoparticle/graphene catalysts were based on published experimental observations, besides those on the preparation of graphenes [33, 34], known procedures were used for immobilization of Pd nanoparticles over the support [36, 37].

3.1 Characterization of the Palladium Nanoparticle/Graphene Catalysts

Figure 2 shows the XRD patterns of GrO, Pd/Gn1, Pd/Gn2 and Pd/Gn3. Since the reflections characteristic of graphite (graphite(002) reflection at 2Θ ≈ 26°) did not appear in the XRD pattern of the GrO sample, oxidation can be considered successful. The reflection characteristic of GrO appeared at 2Θ = 10.3°. Following exfoliation by ultrasound and reduction this peak disappeared, indicating that the GO structure was transformed. Samples exhibited the peak characteristic of graphene at 2Θ ≈ 25°, i.e. a wide and low intensity peak with poorly defined maximum. The Pd(111) reflection (2Θ ≈ 40°) is moderately intensive in the case of Pd/Gn1 and very weak in the pattern of the catalysts prepared by precipitation using Na_2CO_3, which may be due to different size and morphology of the metal particles and/or the oxidation state of the metal surface in the latter materials.

Figure 3 shows the Raman spectra of GrO and the hybrid materials. In the Raman spectrum of GrO two intense bands are observed, one at 1,600 cm^{-1} (G band) corresponding to the in-phase lattice vibration and the disorder induced band at 1,325 cm^{-1} (D band) [24, 38, 39]. The G' band corresponding to two inelastic scattering events involving two-phonons (2,600–2,800 cm^{-1}) was not detected, similarly

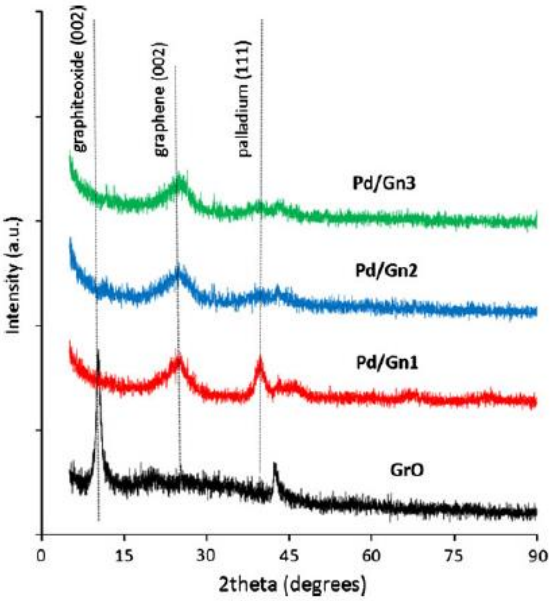

Fig. 2 XRD pattern of GrO and Pd/Gn materials

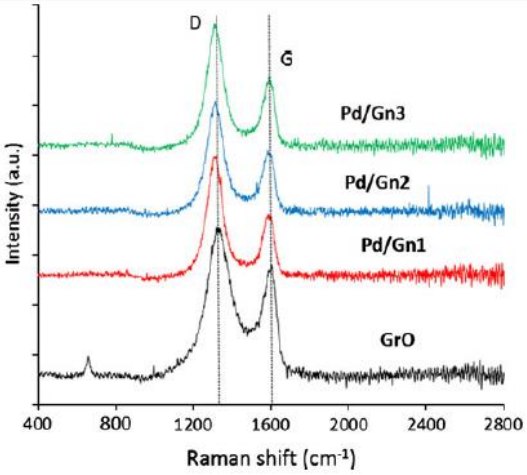

Fig. 3 Raman spectra of GrO and selected Pd/Gns

with the Raman spectra of functionalized graphite [40] or Pd-graphene hybrids prepared previously [39]. The ratio of the intensities of the D and G bands in GrO (I_D/I_G) was 1.33, which increased following reduction and immobilization of Pd nanoparticles to 2.00 (Pd/Gn1), 1.94 (Pd/Gn2) and 1.74 (Pd/Gn3), respectively. This increase may be attributed both to decreases in the size of the graphene sheets and to the chemical interactions of the nanoparticles and the graphene. Furthermore, the slight shift of the G band maxima to lower wavenumbers, i.e. 1,587 cm^{-1} (Pd/Gn1), 1,584 cm^{-1} (Pd/Gn2) and 1,590 cm^{-1} (Pd/Gn3), respectively, when compared to GrO, confirmed the deterioration of the sp^2 carbon ribbons by reduction and metal particle immobilization [39]. Indeed, calculating the in-plane crystallite sizes using the formula $L_a\,(nm) = (2.4 \times 10^{-10})\,\lambda^4\,(I_G/I_D)$ [38] we found a decrease in the size from 66.8 nm (GrO) to 44.4 (Pd/Gn1), 45.8 (Pd/Gn2) and 51.1 (Pd/Gn3) nm, respectively.

The bulk and surface composition of the hybrid materials were determined by ICP-OES and XPS measurements (see Table 1). As expected the metal contents of the samples were higher as the calculated, due to the weight loss of the support during reduction of GrO to Gn. From the comparison of the ICP bulk compositions with values of the surface compositions it is obvious, that the loaded Pd is concentrated on the surface of the multi-layered graphene, together with the Na contamination, left behind after the preparation procedure.

The chemical state of the constituents was determined from the XPS spectra by evaluating the recorded line-shapes of the O 1s, C 1s and Pd 3d spectral ranges. Representative spectra are depicted in Fig. 4 for the Pd/Gn1 sample. The relatively broad peak envelopes were by fitted by three or four Gauss-Lorenz (70:30) type components (1.6–1.8 eV half-widths) of which position were identical (within ±0.2 eV) in all three materials and were assigned based on literature as shown in Table 2 [23, 35, 41, 42]. The Pd 3d doublet peak envelopes were fitted by three pairs of lines separated by 5.25 eV, which were identified as corresponding to the elemental state of Pd; to oxidized Pd, e.g. to a thin oxide layer on the particles; and Pd bonded to an electronegative anion assigned as carboxylic groups. From the peak-synthesis procedure performed for all three samples we evaluated the ratio of the reduced Pd as 53 (Pd/Gn1), 43 (Pd/Gn2) and 49 (Pd/Gn3) atomic%, respectively.

The morphology of the Pd nanoparticle-graphene materials was examined by TEM. Characteristic TEM images with the metal particle size distribution of the hybrid materials as inserts are shown in Fig. 5. Carbon nanosheets are distinguishable in the TEM image of GrO (Fig. 5a), and the nanosheets were also maintained following reduction and Pd immobilization as indicated by the images of Pd/Gns (Fig. 5b–d). The materials exhibiting the most uniform Pd particle distributions over the support are the egg-shell type Pd/Gn2 and Pd/Gn3 catalysts. The Pd particle size distributions are fairly uniform for all three catalysts; the majority of the particles were found to be of 2–5 nm. However, the materials prepared using precipitation by Na_2CO_3 exhibited a narrower Pd size distribution. Thus, Pd/Gn2 and Pd/Gn3 had 83 and 86 % of the particles within 2–4 nm, whereas Pd/Gn1 only 72 %. In the case of the latter material larger Pd particles up to 12 nm were also detected (Fig 5b).

Table 1 Bulk (ICP-OES) and surface (XPS) composition of the Pd nanoparticle/graphene hybrid materials

	Bulk composition (wt%)		Surface composition (wt%)[a]			
Material	Pd	Na	Pd	Na	C	O
Pd/Gn1	6.4	0.2	13.5 (15.4)	1.1 (1.3)	72.9 (83.4)	12.5
Pd/Gn2	5.3	1.2	6.4 (7.4)	2.2 (2.6)	77.6 (90.0)	13.8
Pd/Gn3	5.4	1.1	6.4 (7.4)	1.6 (1.8)	78.5 (90.8)	13.6

[a] In brackets the oxygen omitted surface compositions

3.2 Enantioselective Hydrogenation of α,β-Unsaturated Carboxylic Acids

The Pd/Gns were tested as catalyst in the asymmetric hydrogenation of several prochiral aliphatic α,β-unsaturated carboxylic acids, i.e. **1a**, **2a** and **3a** to the corresponding saturated acids: 2-methylhexanoic acid (**1b**), 2-methylbutanoic acid (**2b**) and 2-methylsuccinic acid (**3b**), using CD as modifier in the absence and the presence of BA additive (Scheme 1.).

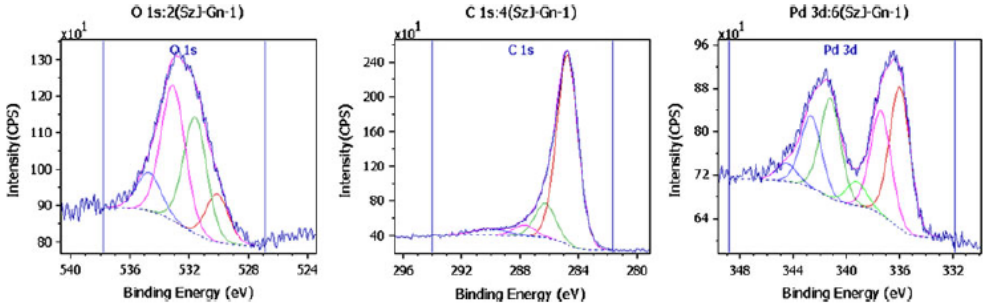

Fig. 4 O 1s, C 1s and Pd 3d region of the XPS spectrum of the Pd/Gn1 material

Table 2 XPS derived surface chemical state of the constituents

Element, line	Chemical shift, BE (eV)	Assignment
Palladium, Pd $3d_{5/2}$	335.9	Pd
	337.5	Pd–O
	339.3	Pd–O–C = O
Carbon, C 1s	284.8	C–C, reference
	286.3	C–O–C
	288.0	O–C = O
	290.3	π–π* satellite
Oxygen, O 1s	530.1	O–Na (O–Pd)
	531.5	O = C
	533.0	C–O–C
	534.5	Adsorbed H_2O

reduced. Moreover, it should also be considered the surface restructuring effect of the chiral modifier [43]. Accordingly, the results should be interpreted with special care and detailed examinations are further needed. The present results are in agreement with earlier studies on the enantioselective hydrogenations of aliphatic unsaturated carboxylic acids over supported Pd catalysts modified by CD, which showed the influence of the particle size and distribution [44]. However, it was also shown that the texture and morphology of the support may also have effect on the enantioselectivity [37, 45]. The use of the achiral amine additive (BA) improved the ee. Surprisingly, the conversions also increased by using BA opposite to the initial rate decrease observed previously over Pd catalysts supported on conventional supports [30, 32], (see entries 2 vs 3; 7 vs 8; 9 vs 10; 11 vs 12; 15 vs 16). Similar tendencies were

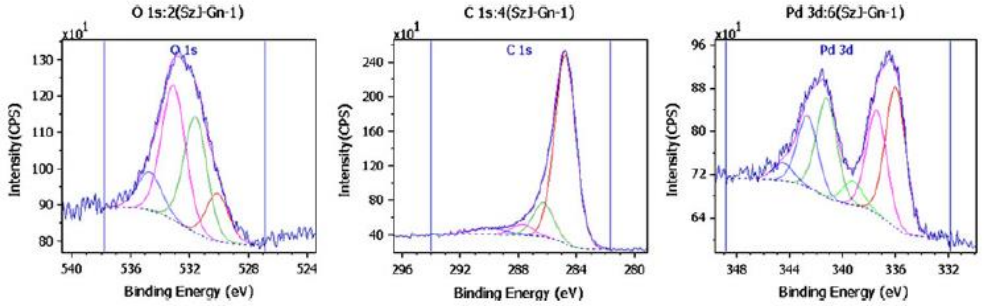

Fig. 4 O 1s, C 1s and Pd 3d region of the XPS spectrum of the Pd/Gn1 material

Table 2 XPS derived surface chemical state of the constituents

Element, line	Chemical shift, BE (eV)	Assignment
Palladium, Pd $3d_{5/2}$	335.9	Pd
	337.5	Pd–O
	339.3	Pd–O–C = O
Carbon, C 1s	284.8	C–C, reference
	286.3	C–O–C
	288.0	O–C = O
	290.3	π–π* satellite
Oxygen, O 1s	530.1	O–Na (O–Pd)
	531.5	O = C
	533.0	C–O–C
	534.5	Adsorbed H_2O

Results obtained under experimental conditions usually applied in the asymmetric hydrogenations of these unsaturated acids [29–32] are summarized in Table 3. In the hydrogenation of monocarboxylic acids we chose toluene as solvent, as the best results in these reactions were reported in hydrocarbons [29, 32]. Hydrogenation of **3a**, however, was studied in methanol, the solvent found most appropriate for this reaction [30].

The data summarized in Table 3 shows that Pd/Gn catalysts were active in the hydrogenation of the α,β-unsaturated carboxylic acids tested. The highest optical yield was achieved in the hydrogenation of **1a** over Pd/Gn1. This catalyst provided higher enantioselectivities as compared with the commercial Pd/C as well; both in presence and absence of BA (see entries 2 and 3, respectively). Catalysts Pd/Gn2 and Pd/Gn3 produced lower ee values. The higher activity and enantioselectivity of Pd/Gn1 calls attention to the influence of the Pd particle size, morphology and surface valence state of the metal. However, it should be mentioned, that the hydrogenation are preceded by prehydrogenations of the catalysts in the corresponding solvent, thus one may presume that before the reactions the surface oxide layer of the pristine materials is further reduced. Moreover, it should also be considered the surface restructuring effect of the chiral modifier [43]. Accordingly, the results should be interpreted with special care and detailed examinations are further needed. The present results are in agreement with earlier studies on the enantioselective hydrogenations of aliphatic unsaturated carboxylic acids over supported Pd catalysts modified by CD, which showed the influence of the particle size and distribution [44]. However, it was also shown that the texture and morphology of the support may also have effect on the enantioselectivity [37, 45]. The use of the achiral amine additive (BA) improved the ee. Surprisingly, the conversions also increased by using BA opposite to the initial rate decrease observed previously over Pd catalysts supported on conventional supports [30, 32], (see entries 2 vs 3; 7 vs 8; 9 vs 10; 11 vs 12; 15 vs 16). Similar tendencies were observed on all three graphene supported catalysts, thus, the effect may be attributed to the special properties of the graphene support, which may influence the interaction strength of the amine, unsaturated acid and the acid-modifier salt with the metal surface. However, the graphene support did not changed the effect of the acid structure on the hydrogenation results, as the present study on the structure of the acid (using the above mentioned three acids) showed similar influence as described over conventional catalysts, i.e. the increase in length of the β substituent increased the ee and decreased the rate [46].

Increasing the concentration of CD reduced the conversion (entries 1, 3, 4) and at the same time enhanced the enantioselectivity up to the use of 5 mol% CD (compared to the acid amount). At this CD concentration the reaction is not yet slowed down significantly and at the same time maximum ee can be achieved. Increasing the H_2 pressure increased both conversion and ee (entries 3, 5, 6). Variations in the hydrogenation conditions (temperature, H_2 pressure, CD concentration, BA concentration) allow concluding that the optical yield presumably can be further increased depending on the acid structure; further investigations will be carried out and will be reported in due

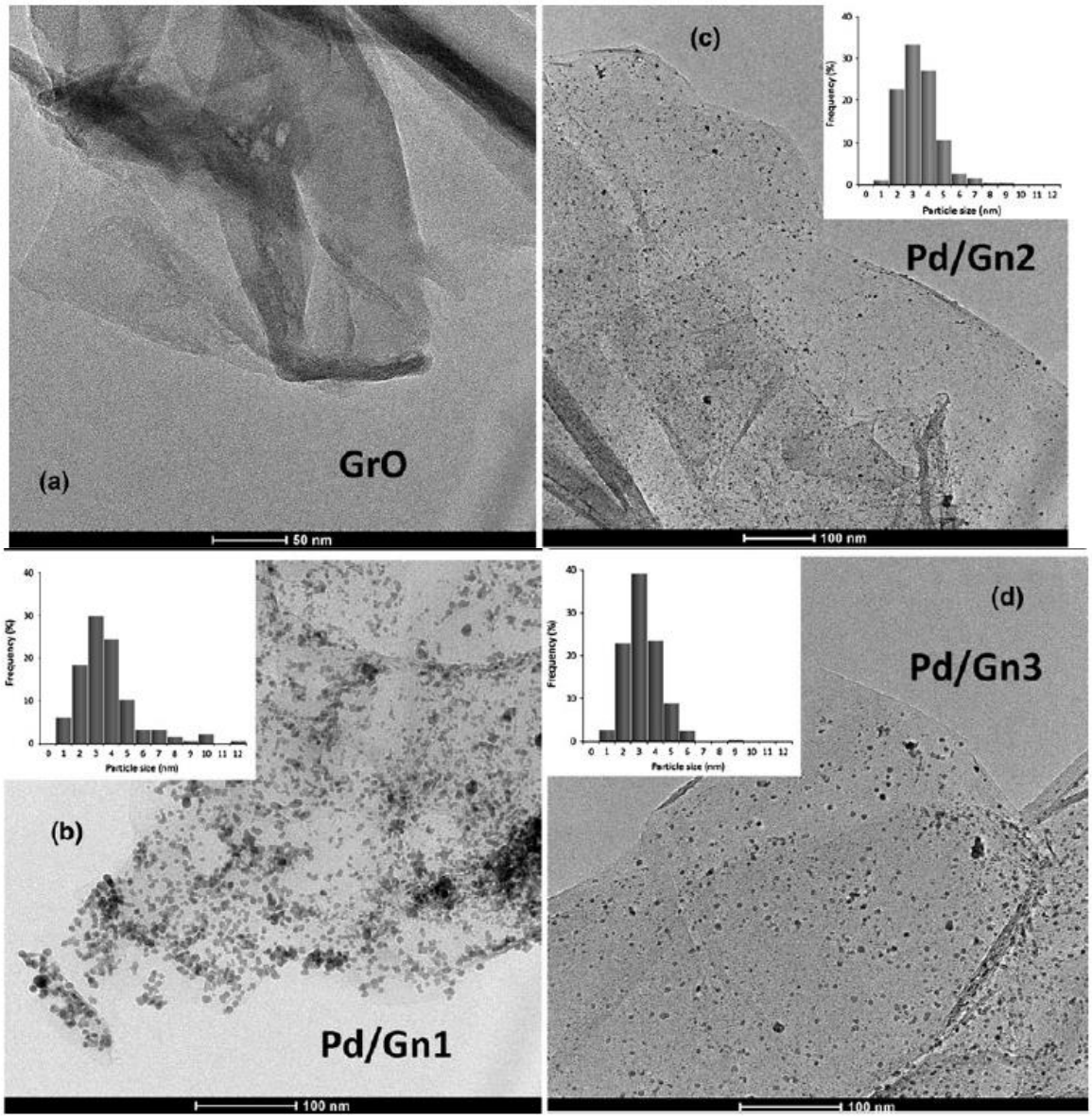

Fig. 5 TEM images of GrO and Pd/Gns, Pd particle size distributions are shown as inserts

Scheme 1 Scheme of hydrogenation of the selected α,β-unsaturated carboxylic acids over CD-modified Pd/Gns

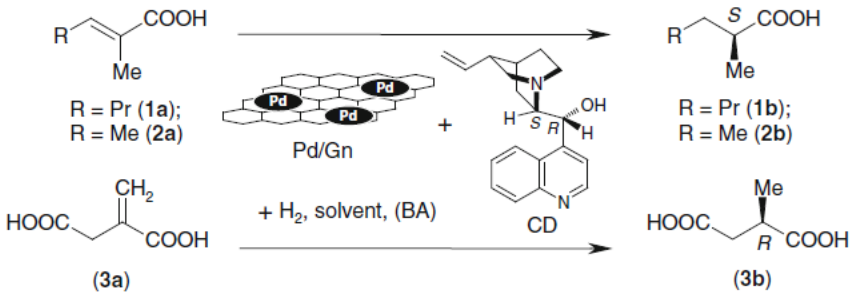

course. It is also noted that following our present investigation, which proves the applicability of Pd/graphene hybrid materials in hydrogenations, further development in the material preparation may result in tuning its properties for specific applications including the enantioselective hydrogenation of prochiral activated olefins.

Table 3 Asymmetric hydrogenations of α,β-unsaturated carboxylic acids over Pd nanoparticle/graphene hybrid materials modified by CD

Entry	Catalyst	Substrate	p H_2 (MPa)	Amount CD (mmol)	Amount BA (mmol)	Conversion (%)	ee[a] (%)
1	Pd/Gn1	**1a**	5	0.025	1	83	43 (*S*)
2	Pd/Gn1	**1a**	5	0.05	0	41	39; 27[b] (*S*)
3	Pd/Gn1	**1a**	5	0.05	1	72	47; 42[b] (*S*)
4	Pd/Gn1	**1a**	5	0.1	1	68	47 (*S*)
5	Pd/Gn1	**1a**	1	0.05	1	56	38 (*S*)
6	Pd/Gn1	**1a**	10	0.05	1	89	49 (*S*)
7	Pd/Gn2	**1a**	5	0.05	0	4	12 (*S*)
8	Pd/Gn2	**1a**	5	0.05	1	33	31 (*S*)
9	Pd/Gn3	**1a**	5	0.05	0	11	26 (*S*)
10	Pd/Gn3	**1a**	5	0.05	1	49	29 (*S*)
11	Pd/Gn1	**2a**	5	0.05	0	75	32 (*S*)
12	Pd/Gn1	**2a**	5	0.05	1	100	40 (*S*)
13	Pd/Gn2	**2a**	5	0.05	0	100	12 (*S*)
14	Pd/Gn2	**2a**	5	0.05	1	100	16 (*S*)
15	Pd/Gn3	**2a**	5	0.05	0	55	14 (*S*)
16	Pd/Gn3	**2a**	5	0.05	1	90	16 (*S*)
17[c]	Pd/Gn1	**3a**	2	0.05	0	100	3 (*R*)
18[c]	Pd/Gn1	**3a**	2	0.05	1	100	10 (*R*)
19[c]	Pd/Gn1	**3a**	2	0.05	2	100	14 (*R*)
20[c]	Pd/Gn2	**3a**	2	0.05	2	100	11 (*R*)
21[c]	Pd/Gn3	**3a**	2	0.05	2	100	13 (*R*)

Reaction conditions: 15 mg catalyst, 1 mmol substrate, 297 K, 10 cm^3 toluene, hydrogenation time 1.5 h

[a] Configuration of the excess enantiomer in brackets

[b] Enantioselectivities obtained by using Pd/C 10 % (Fluka, 75990) catalyst

[c] 30 min hydrogenations in 10 cm^3 methanol

4 Conclusion

Although reports on the hydrogenating activities of Pd/Gn catalysts have been published before this study [47, 48], to our best knowledge experimental observations regarding their utilization in asymmetric reactions, including hydrogenations, have not been reported yet. According to our data described above, Pd/Gn catalysts synthesized in our laboratory by co-reduction of palladium and graphite oxide using $NaBH_4$ are active in the asymmetric hydrogenation of aliphatic α,β-unsaturated carboxylic acids in the presence of cinchonidine modifier. Best results were obtained using BA as additive, which besides improving the ee also increased the conversion. The special properties of the graphene support was assumed to be at the origin of this surprising rate increase, due to its influence on the interaction strength of the amine, unsaturated acid and the acid-modifier salt with the metal surface. Elucidation of the reason of the effect of the graphene support, however, necessitates further studies, which could be of great importance in designing novel and more efficient heterogeneous catalysts for asymmetric hydrogenations.

Acknowledgments Financial support by the Hungarian National Science Foundation (OTKA Grant K 72065) and TÁMOP-4.2.2.A-11/1/KONV-2012-0047 are highly appreciated.

References

1. Smith GV, Notheisz F (1999) Heterogeneous catalysis in organic chemistry. Academic Press, San Diego
2. Sheldon RA, van Bekkum H (2001) Fine chemicals through heterogeneous catalysis. Wiley-VCH, Weinheim
3. Dörwald FZ (ed) (2002) Organic synthesis on solid phase. Wiley-VCH, Weinheim
4. Ding K, Uozumi Y (eds) (2008) Handbook of asymmetric heterogeneous catalysis. Wiley-VCH, Weinheim
5. Rylander P (1979) Catalytic hydrogenation in organic syntheses. Academic Press, New York
6. Bartók M, Czombos J, Felföldi K, Gera L, Göndös Gy, Molnár Á, Notheisz F, Pálinkó I, Wittmann Gy, Zsigmond ÁG (1985) Stereochemistry of heterogeneous metal catalysis. Wiley, Chichester
7. Nishimura S (2001) Handbook of heterogeneous catalytic hydrogenation for organic synthesis. Wiley, New York
8. Molnár Á, Smith GV, Bartók M (1986) J Catal 101:67
9. Molnár Á, Smith GV, Bartók M (1989) Adv Catal 36:329
10. Molnár Á, Katona T, Bartók M, Varga K (1991) J Mol Catal 64:41

11. Bartók M, Szőllősi Gy, Mastalir A, Dékány I (1999) J Mol Catal A Chem 139:227
12. Balázsik K, Török B, Szakonyi G, Bartók M (1999) Appl Catal A Gen 182:53
13. Mastalir Á, Király Z, Szőllősi Gy, Bartók M (2000) J Catal 194:146
14. Kun I, Szőllősi G, Bartók M (2001) J Mol Catal A Chem 169:235
15. Molnár Á, Mastalir Á, Bartók M (1989) J Chem Soc Chem Commun 124
16. Sirokmán G, Mastalir Á, Molnár Á, Bartók M, Schay Z, Guczi L (1990) Carbon 28:35
17. Notheisz F, Mastalir Á, Bartók M (1992) J Catal 134:608
18. Mastalir Á, Notheisz F, Bartók M, Haraszti T, Király Z, Dékány I (1996) Appl Catal A Gen 144:237
19. Mastalir A, Király Z, Walter J, Notheisz F, Bartók M (2001) J Mol Catal A Chem 175:205
20. Novoselov KS, Geim AK, Morozov SV, Jiang D, Zhang Y, Dubonos SV, Grigorieva IV, Firsov AA (2004) Science 306:666
21. Yang WR, Ratinac KR, Ringer SP, Thordarson P, Gooding JJ, Braet F (2010) Angew Chem Int Ed 49:2114
22. Brownson DAC, Kampouris DK, Banks CE (2011) J Power Sources 196:4873
23. Antolini E (2012) Appl Catal B Environ 123–124:52
24. Machado BF, Serp P (2012) Catal Sci Technol 2:54
25. Klabunovskii E, Smith GV, Zsigmond Á (2006) Heterogeneous enantioselective hydrogenation. Springer, Dordrecht
26. Mallat T, Orglmeister E, Baiker A (2007) Chem Rev 107:4863
27. Bartók M (2010) Chem Rev 110:1663
28. Margitfalvi JL, Tálas E (2010) Catalysis 22:144
29. Szőllősi Gy, Hanaoka T, Niwa S, Mizukami F, Bartók M (2005) J Catal 231:480
30. Szőllősi G, Balázsik K, Bartók M (2007) Appl Catal A Gen 319:193
31. Szőllősi Gy, Németh Zs, Hernádi K, Bartók M (2009) Catal Lett 132:370
32. Makra Zs, Szőllősi Gy, Bartók M (2012) Catal Today 181:56
33. Hummers WS, Offeman RE (1958) J Am Chem Soc 80:1339
34. Yang J, Tian CG, Wang L, Fu HG (2011) J Mater Chem 21:3384
35. Moulder JF, Stickle WF, Sobol PE, Bomben KD (1992) Handbook of X-ray photoelectron spectroscopy. Perkin-Elmer Corp, Eden Prairie
36. Hu Z-L, Aizawa M, Wang Z-M, Yoshizawa N, Hatori H (2010) Langmuir 26:6681
37. Kubota T, Ogawa H, Okamoto Y, Misaki T, Sugimura T (2012) Appl Catal A Gen 437–438:18
38. Pimenta MA, Dresselhaus G, Dresselhaus MS, Cancado LG, Jorio A, Saito R (2007) Phys Chem Chem Phys 9:1276
39. Li Y, Fan X, Qi J, Ji J, Wang S, Zhang G, Zhang F (2010) Nano Res 3:429
40. Chakraborty S, Guo W, Hauge RH, Billups WE (2008) Chem Mater 20:3134
41. Yang D, Velamakanni A, Bozoklu G, Park S, Stoller M, Piner RD, Stankovich S, Jung I, Field DA, Ventrice CA, Ruoff RS (2009) Carbon 47:145
42. Tkachev SV, Buslaeva EYu, Naumkin AV, Kotova SL, Laure IV, Gubin SP (2012) Inorg Mater 48:796
43. Hess R, Krumeich F, Mallat T, Baiker A (2004) Catal Lett 92:141
44. Nitta Y, Kubota T, Okamoto Y (2004) J Mol Catal A Chem 212:155
45. Impalá D, Franceschini S, Piccolo O, Vaccari A (2008) Catal Lett 125:243
46. Szőllősi Gy, Niwa S, Hanaoka T, Mizukami F (2005) J Mol Catal A Chem 230:91
47. He HK, Gao C (2011) Sci China Chem 54:397
48. Chandra S, Bag S, Das P, Bhattacharya D, Pramanik P (2012) Chem Phys Lett 519–520:59